PNAS RESEARCH ARTICLE | IMMUNOLOGY AND INFLAMMATION

AIM2 sensors mediate immunity to *Plasmodium* infection in hepatocytes

Camila Marques-da-Silva[a,b,1], Barun Poudel[c,1], Rodrigo P. Baptista[b,d], Kristen Peissig[a,b], Lisa S. Hancox[e], Justine C. Shiau[b,f], Lecia L. Pewe[e], Melanie J. Shears[g,h], Thirumala-Devi Kanneganti[i], Photini Sinnis[g,h], Dennis E. Kyle[a,b,f], Prajwal Gurung[c,j], John T. Harty[e,j], and Samarchith P. Kurup[a,b,2]

Edited by Katherine Fitzgerald, University of Massachusetts Medical School, Worcester, MA; received June 15, 2022; accepted November 18, 2022

Malaria, caused by *Plasmodium* parasites is a severe disease affecting millions of people around the world. *Plasmodium* undergoes obligatory development and replication in the hepatocytes, before initiating the life-threatening blood-stage of malaria. Although the natural immune responses impeding *Plasmodium* infection and development in the liver are key to controlling clinical malaria and transmission, those remain relatively unknown. Here we demonstrate that the DNA of *Plasmodium* parasites is sensed by cytosolic AIM2 (absent in melanoma 2) receptors in the infected hepatocytes, resulting in Caspase-1 activation. Remarkably, Caspase-1 was observed to undergo unconventional proteolytic processing in hepatocytes, resulting in the activation of the membrane pore-forming protein, Gasdermin D, but not inflammasome-associated proinflammatory cytokines. Nevertheless, this resulted in the elimination of *Plasmodium*-infected hepatocytes and the control of malaria infection in the liver. Our study uncovers a pathway of natural immunity critical for the control of malaria in the liver.

Malaria | innate immunity | Caspase-1 | liver

Significance

Clinical malaria caused by *Plasmodium* parasites is responsible for the death and suffering of millions of people around the world. While humans are known to mount protective innate immune responses against *Plasmodium* during the course of its initial development in the liver, we understand little about the mechanism of this process. This knowledge gap has hindered our ability to exploit natural immune responses to combat malaria. We show that DNA molecules of *Plasmodium* parasites are detected by AIM2 receptors present in host hepatocytes, leading to unconventional processing of Caspase-1 and activation of the inflammasome pathway. This results in programmed cell-death of the hepatocytes harboring *Plasmodium* and early control of the infection in the liver itself, potentially limiting clinical malaria.

Malaria is a devastating disease that affects over 200 million people each year (1). *Plasmodium* parasites that cause malaria undergo an asymptomatic phase of obligatory development and replication in the hepatocytes that lasts for approximately 7 days in humans (the preerythrocytic 'liver-stage'), before advancing to the disease-causing 'blood-stage' of the infection, where they infect the red blood cells (2). Considering that the maturation of *Plasmodium* in the liver is a prerequisite for clinical malaria and transmission, the liver-stage is also the favored target for antimalarial vaccinations and therapies (3–6). Natural immune responses that impede *Plasmodium* infection in the liver are considered to limit the development and impact of blood-stage malaria (7–12). Therapeutically targeting such host responses, rather than *Plasmodium* itself which is more genetically flexible, would reduce the likelihood of emergence of new drug resistance, which has been a major challenge in our fight against malaria (6). In addition, *P. vivax* is known to establish long-term dormant infections in hepatocytes, enabling them to seed sporadic relapse infections for years (13). Enhancing innate immune responses in the liver would eliminate such dormant parasites, preventing relapse infections. Although various innate immune pathways stimulated by *Plasmodium* in its blood-stage are currently known, such responses are not induced until several days after the initiation of an infection, and would have minimal impact on the early control of natural infections or the resultant clinical disease (14). Thus, filling the knowledge gap in our understanding of the innate immune responses directed at *Plasmodium* in the liver is a critical step in our fight against malaria.

A defining component of innate immunity in vertebrates is the response to pathogen-associated molecular patterns (PAMPs) that are recognized through germline-encoded pattern recognition receptors (PRRs) expressed in host cells (15, 16). Although host genetics and natural immunity are known to offer resistance to malaria in humans, the immune pathways that hinder *Plasmodium* infection of the liver, specifically in hepatocytes, remain relatively unknown (14, 17, 18). Currently, the only pathway of natural immunity known to curb malaria infection in the liver is driven by melanoma differentiation-associated protein 5 receptors in the hepatocyte cytosol, which sense *Plasmodium* RNA to induce type I interferon (IFN) responses (8, 10, 14). Strong type I IFN responses are known to enhance the control of *Plasmodium* in the liver, resulting in delayed onset of blood-stage malaria, reduced parasitemia levels, and improved survival in mice (7, 12). This suggests that the identification of innate immune responses that control malaria in the liver would be of immense translational value.

It is unlikely that RNA is the only *Plasmodium*-derived PAMP that gains access to the hepatocyte cytosol, or would be the sole driver of innate immune responses in the liver. Various intracellular bacterial, fungal, and protozoal PAMPs are sensed by PRRs in the cytoplasm of host cells to induce the formation of 'inflammasomes' (19–24). Inflammasomes

Author contributions: C.M.-d.-S., B.P., R.P.B., K.P., J.C.S., P.S., P.G., J.T.H., and S.P.K. designed research; C.M.-d.-S., B.P., K.P., L.S.H., J.C.S., L.L.P., M.J.S., and S.P.K. performed research; T.-D.K. and D.E.K. contributed new reagents/analytic tools; R.P.B. analyzed data; and J.T.H. and S.P.K. wrote the paper.

The authors declare no competing interest.

This article is a PNAS Direct Submission.

[1]C.M.-d.-S. and B.P. contributed equally to this work.

[2]To whom correspondence may be addressed. Email: samar@uga.edu.

This article contains supporting information online at https://www.pnas.org/lookup/suppl/doi:10.1073/pnas.2210181120/-/DCSupplemental.

Published January 3, 2023.

are discrete macromolecular enzymatic complexes formed in the cytosol constituted by PAMP-bound PRRs, procaspase-1, and in some cases, the ASC (apoptosis-associated speck-like protein containing a CARD) adaptor molecules (19, 25). Autoproteolytic cleavage of the procaspase-1 precursor molecule (p46) into its constituent CARD (caspase activation and recruitment domain), p20 and p10 domains occurs at these inflammasome complexes, and results in the catalytically functional hetero-trameric Caspase-1, composed of the p20 and p10 subunits (26, 27). Activated Caspase-1 in turn facilitates the elimination of pathogens by inducing programmed death (pyroptosis) in host cells through proteolytic activation of the membrane pore-forming protein, Gasdermin D (GSDMD). Additionally, the inflammasome complex also activates the proinflammatory cytokines interleukin (IL)-1 and IL-18 to alert the immune system more broadly (28–30). Of note, this current model for Caspase-1 activation dynamics has been established based on studies in immune cells such as macrophages or monocytes, or neoplastic cell-lines (19, 31). The mechanisms or consequences of Caspase-1 activation in parenchymal cells or nonimmune cells such as hepatocytes have rarely been investigated, despite their potential relevance to the innate immune-surveillance mechanisms in tissues and the global inflammatory responses of the host (32, 33).

We surmised that a comprehensive screen for transcriptional perturbations in hepatocytes infected with *Plasmodium* would offer insights into the innate immune responses elicited by *Plasmodium* infection in the liver. Here, we use single-cell RNA (scRNA) sequencing in primary human hepatocytes infected with the most important human malaria parasite, *Plasmodium falciparum*, to reveal a concerted upregulation of transcripts associated with the programmed cell-death and inflammasome pathways. Using biochemical approaches and *in vivo* studies in mice, we demonstrate that AIM2 receptors in *Plasmodium*-infected hepatocytes detect *Plasmodium* DNA to induce inflammasome-mediated Caspase-1 activation. Although Caspase-1 was observed to undergo noncanonical proteolytic processing in *Plasmodium*-infected hepatocytes, it resulted in GSDMD-mediated pyroptotic cell-death and control of malaria in the liver itself.

Results

Inflammasome-Mediated Caspase-1 Activation in *Plasmodium*-Infected Hepatocytes. To gain an unbiased and comprehensive understanding of the innate immune responses elicited by *Plasmodium* parasites in hepatocytes, we determined the total transcriptional changes in primary human hepatocytes infected with *P. falciparum* (*Pf*) using scRNA sequencing. Primary human hepatocytes were employed specifically to gain access to the full range of biochemical perturbations in response to *Pf* infection, considering that the immortalized or neoplastic cell-lines that have been relied on in the past for similar purposes are known to have fundamentally altered immune, cell-death, and metabolic pathways (34–36). Primary human hepatocytes were infected with a field isolate of *Pf* sporozoites obtained from infected mosquitoes, and scRNA sequencing was performed on infected and uninfected hepatocytes (*SI Appendix*, Fig. S1*A* and Fig. 1*A*). The *Pf*-infected hepatocytes were identified bioinformatically from the sequence reads using *Pf*-specific transcripts, and compared with the uninfected hepatocytes derived from the same culture (Fig. 1 *B* and *C*). Our experimental approach normalized each cell to environmental exposures such as any mosquito or salivary gland–derived debris, while reliably distinguishing infected and uninfected cells. The *Pf*-infected and -uninfected hepatocytes clustered separately in principal component analysis, signifying their discrete transcriptional profiles (Fig. 1*B*). Gene set enrichment analyses indicated that various genes pertinent to cell-injury, cell-invasion, and acute phase responses in the host were transcriptionally perturbed in *Pf*-infected hepatocytes (*SI Appendix*, Fig. S1 *B–D*). Canonical pathway analysis and the enrichment of functional molecular interactions indicated that liver cell-damage responses, programmed cell-death pathways, and inflammatory responses in hepatocytes were the key immune processes impacted, admitting the possibility of the induction of the inflammasome pathway in *Plasmodium*-infected hepatocytes (Fig. 1*D*). Corroborating this finding, we observed broad transcriptional changes in a variety of genes of the inflammasome pathway (Fig. 1*E*). Of note, hepatocytes are known to upregulate the expression of its cytoplasmic PRRs such as NLRP(Nucleotide-binding oligomerization domain) 3, AIM2 etc., as well as the proinflammatory cytokine IL-1β following PAMP stimulation and the induction of the inflammasome pathway (37). In support of the above foundational data, we observed the presence of inflammasome complexes containing Caspase-1 associated with human hepatocytes infected with *Pf* (Fig. 2*A*). Of note, above cryosections were prepared from *Pf*-infected liver-humanized mice, where the infection is limited to the hepatocytes of human origin embedded in the mouse liver. The data also signify the potential existence of the inflammasome pathway in vivo. It is also noteworthy that in many instances, we observed that Caspase-1 containing inflammasomes were generated proximal to the early developmental stages of *Plasmodium* parasites in both human and mouse hepatocytes (*SI Appendix*, Fig. S1*E*), offering stark similarity to the inflammasomes formed in response to the detection of DNA from intracellular bacterial pathogens in myeloid cells (38, 39). Taken together, these data suggested that inflammasome-mediated Caspase-1 activation occurs in hepatocytes in response to *Plasmodium* infection.

AIM2 Facilitates Caspase-1-Mediated Control of Liver-Stage Malaria. Although *Pf* is the deadliest and the most widespread species of *Plasmodium* affecting humans, they do not productively infect mouse hepatocytes. Therefore, we employed the mouse malaria parasite, *Plasmodium yoelii* (*Py*) to mechanistically and feasibly dissect the immunobiology of liver-stage malaria using in vitro or in vivo studies. The pathogenesis of *Py* in mice resembles that of *Pf* in humans in many respects (40). To determine the innate immune signaling pathways in hepatocytes responding to *Plasmodium* infection, we established a murine primary hepatocyte culture model. Here, primary hepatocytes isolated from mice (*SI Appendix*, Fig. S2*A*) were coincubated with sporozoites purified from the salivary glands of *Py*-infected mosquitos (*SI Appendix*, Fig. S2*B*). Such sporozoites were also used for intravenous inoculation into mice for in vivo experiments.

To determine how Caspase-1 activation in hepatocytes impacted the control of liver-stage malaria, we infected Caspase-1/11 deficient (Casp1/11KO (41)), or wild-type C57BL/6 (B6) mice with *Py* sporozoites derived from mosquitoes, and examined the resultant parasite burdens in the liver. Casp1/11KO mice exhibited significantly higher levels of *Py* 18S rRNA in the liver, suggesting that Caspase-1/11 aided in controlling *Plasmodium* infection in its preerythrocytic stage (Fig. 2*B*). In agreement with our finding that Caspase-1 activation in *Py*-infected hepatocytes was dependent on the adaptor molecule, ASC (PYCARD) (*SI Appendix*, Fig. S2*C*), genetic deficiency of ASC resulted in suboptimal control of liver-stage malaria (Fig. 2*B*). Considering that Casp1/11KO mice are also deficient in Caspase-11 in addition to Caspase-1, we sought to determine the extent to which Caspase-11 impacted the control of *Plasmodium* in hepatocytes. Caspase-11 was not activated by *Py* infection in the hepatocytes, nor influenced *Py* control in the liver (*SI Appendix*, Fig. S2 *D–F*).

ASC being a vital component of *Py* control in the liver indicated that *Plasmodium* parasites in hepatocytes are likely detected by

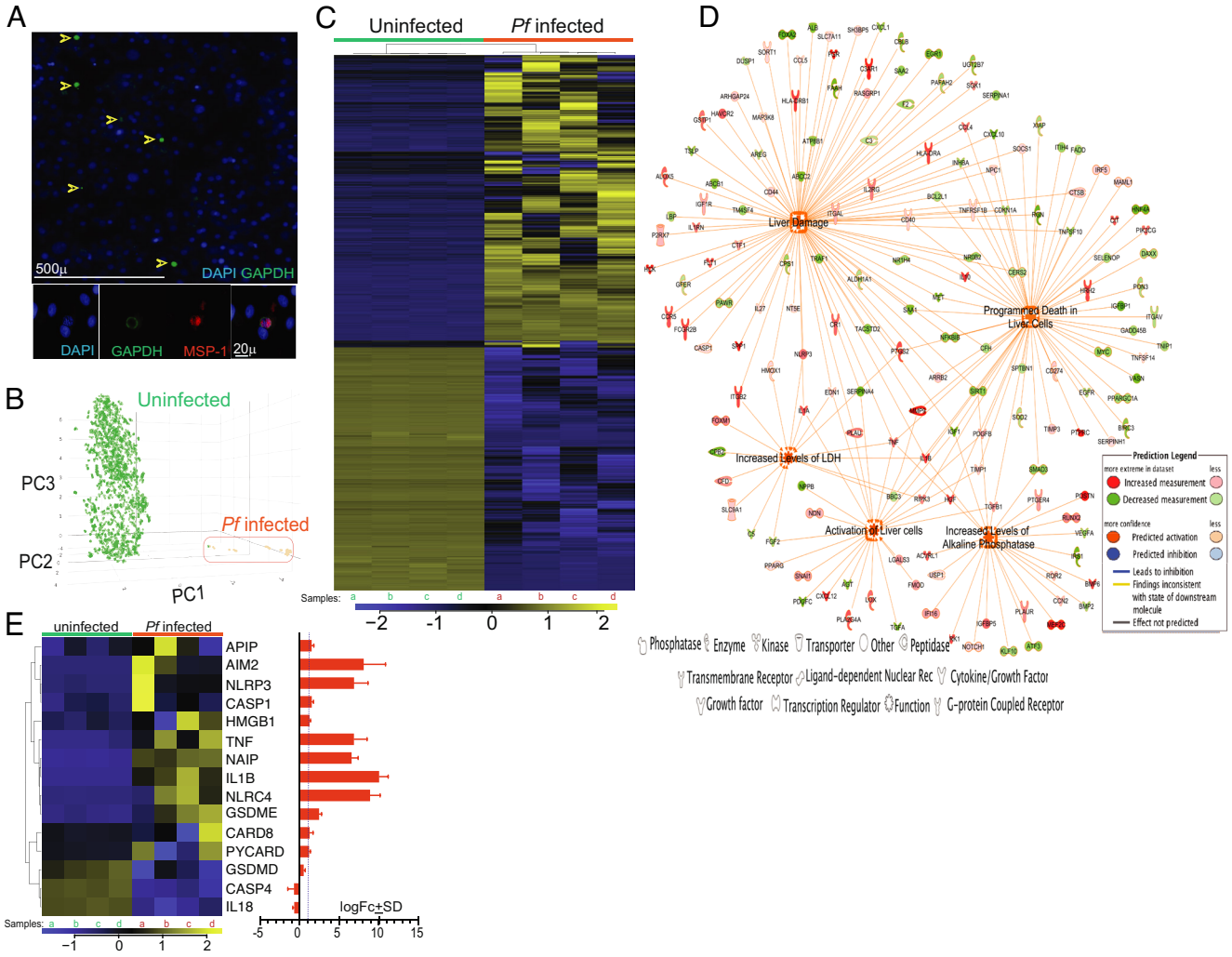

Fig. 1. *P. falciparum* infection induces inflammatory cell-death pathways in hepatocytes. (*A*) Representative pseudocolored fluorescent micrographs showing in vitro cultured primary human hepatocytes infected with *Pf*, 4 d p.i. The individual panels show staining with separate *Pf*-specific antibodies (GAPDH and merozoite surface protein-1, MSP-1) or DNA (DAPI), and fluorescence overlays. MSP-1 expression represents the liver-stage of *Pf*. (*B* and *C*) Transcriptional differences determined by scRNA sequencing of *Pf*-infected or uninfected primary human hepatocytes at 4 d p.i. *Pf*-infected hepatocyte transcripts were plotted for principal component analysis, which corroborated the unsupervised clustering of hepatocytes based on gross transcriptional changes (*B*) or as heat map to depict gross transcriptional differences (*C*). (*D*) Significantly enriched network of functional interactions evaluated by gene-set and biochemical pathway enrichment analysis comparing *Pf*-infected and uninfected human hepatocytes. The nodes represent the key functional outcomes predicted based on the transcriptional identity (represented by color coded proteins, see legend) of the *Pf*-infected primary human hepatocytes at 4 d p.i. (*E*) Heat map depicting transcriptional differences in the genes of the canonical inflammasome pathway determined to be up-regulated by unbiased biochemical pathway enrichment analysis in primary human hepatocytes, maintained ex vivo and coincubated with *Pf* for 4 d. The bar graph on right shows log fold change ± SD (logFC ± SD) in the differential expression of the indicated genes. Dotted line represents logFc of 1. (*C* and *E*) Data obtained from a total of four replicate infections (samples a–d). See *SI Appendix*, Fig. S1*A* for experimental details.

one or more of the ASC-limited PRRs: NLRP3, NLRP1b, (NLR family CARD domain containing 4) NLRC4, or AIM2 (19). In order to delineate the contributions of these innate sensors in the control of liver-stage malaria, we compared *Py* infections in B6 or NLRP3-, NLRP1b-, NLRC4-, or AIM2- deficient mice. AIM2KO mice exhibited significantly higher *Py* burdens in the liver, suggesting that Caspase-1 activation in hepatocytes in response to *Plasmodium* infection is likely mediated by AIM2 sensors (Fig. 2*C*).

Though only the hepatocytes are known to support *Plasmodium* replication and development in the liver, various hematopoietic cells such as the dendritic cells can acquire *Plasmodium* in the liver, skin, or lymphoid organs (9, 42). It is worth highlighting that inflammasome pathways have been characterized almost exclusively in antigen presenting cells (APCs) (25, 32), with little to nothing known about how this pathway operates in parenchymal cells such as the hepatocytes. To assess the extent to which Caspase-1 or AIM2 in hematopoietic cells might contribute to the control of liver-stage malaria, we generated reciprocal bone-marrow chimeric mice using B6, Casp1/11KO, or AIM2KO mice. Quantitation of *Py* infections in these mice indicated that the lack of Caspase-1 or AIM2 expressed in hematopoietic cells did not impact the control of liver-stage malaria (Fig. 2 *D* and *E*). These data indicated that AIM2-mediated Caspase-1 activation in hepatocytes facilitates the control of *Plasmodium* in the liver.

AIM2 Sensors Detect *Plasmodium* DNA in the Infected Hepatocytes. The only known ligand for AIM2 in host cells is double-stranded (ds) DNA of either the host or pathogen origin (27). We hypothesized that *Plasmodium*-derived dsDNA is directly sensed by AIM2 receptors in the infected hepatocytes. To objectively test the interaction between AIM2 sensors and *Plasmodium* dsDNA, as a proof of concept, we first determined whether AIM2 can be coimmunoprecipitated with Bromodeoxyuridine

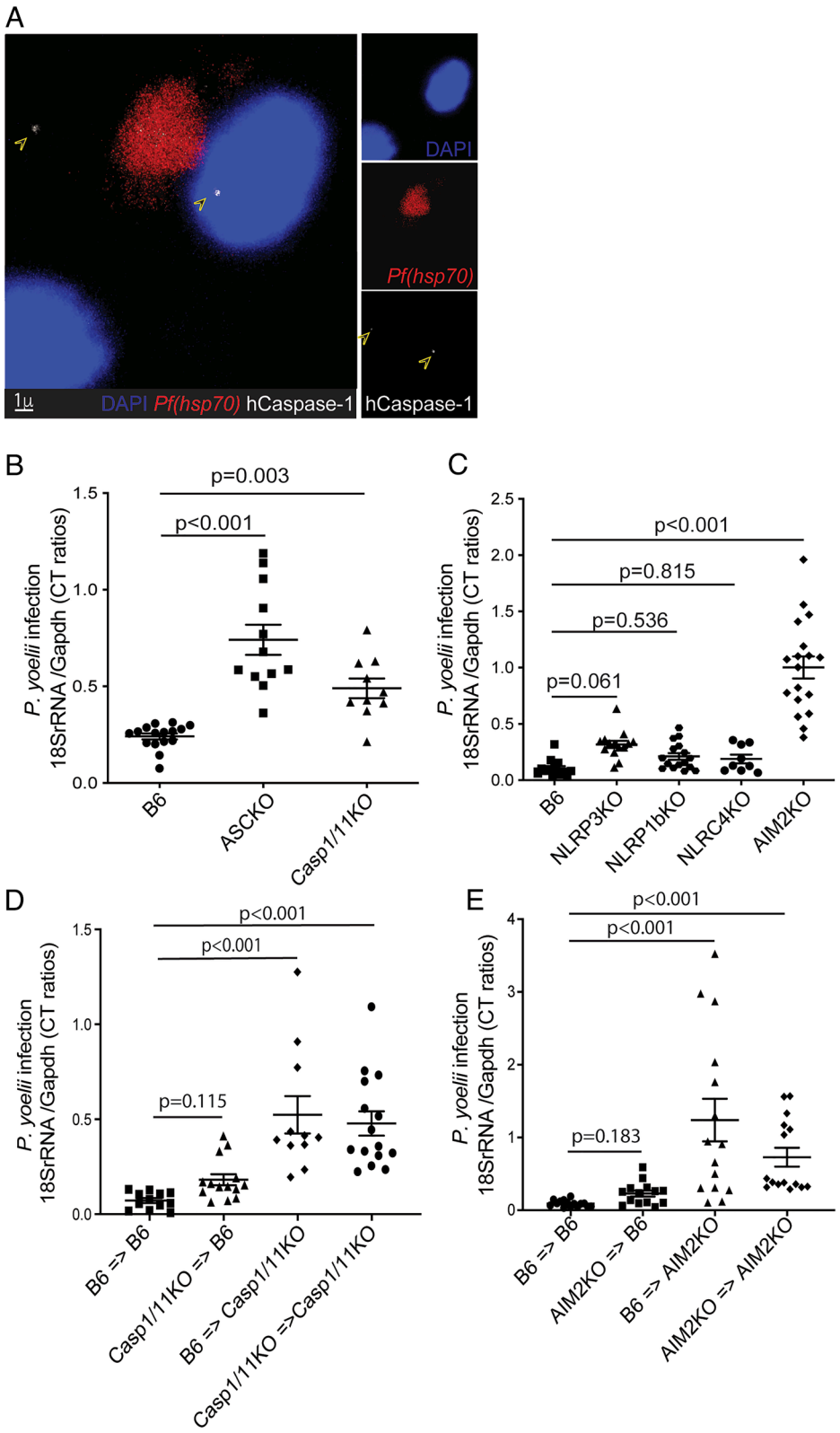

Fig. 2. AIM2-Caspase-1 axis drives the control of liver-stage malaria. (*A*) Representative (of >10 cryosections) pseudocolored confocal image depicting Caspase-1 aggregates (arrows) in human hepatocytes in the liver of a humanized mouse inoculated with *Pf* (30 h p.i). Stained using DAPI for nucleus, hsp70 for *Pf*, and anti-hCaspase-1 antibody. Frequency (%) of association of *Pf* and hCaspase-1: 82.05 ± 2.69. Data presented as mean ± SEM compiled from ≥10 cryosections. Hsp70: heat shock protein 70. (*B* and *C*) Scatter plots showing relative liver-parasite burdens in the indicated mice inoculated with *Py*, at 36 h p.i. (*D*) Scatter plots showing relative parasite burdens at 36 h p.i in the whole livers of B6 or Casp1/11KO chimeric recipient mice reconstituted with B6 or Casp1/11KO bone-marrow and inoculated with *Py* i.v. (*E*) Scatter plots showing relative whole-liver parasite burdens at 36 h p.i. in B6 or AIM2KO chimeric recipient mice reconstituted with B6 or AIM2KO bone-marrow and inoculated with *Py* i.v. (*B–E*) The dots in the scatter plots represent individual mice, with the data combined from 3 separate replicate experiments and presented as mean ± SEM and analyzed using ANOVA with Dunnett's corrections, yielding the indicated *P* values.

(BrdU)-incorporated DNA that has gained access to hepatocyte cytosol. Anti-BrdU-mediated pulldown of BrdU$^+$ DNA obtained from mammalian cells and transfected into primary hepatocytes reliably coimmunoprecipitated AIM2 (*SI Appendix*, Fig. S3*A*). To query the possibility of the direct association of *Plasmodium* DNA and hepatocyte AIM2, we incorporated BrdU into the DNA of *P. berghei* (*Pb*) sporozoites. BrdU is known to integrate into the DNA of in vitro cultured *Pf* that replicate in an environment replete with BrdU (43, 44). However, to generate sporozoite stages with BrdU-incorporated DNA, we reared *Pb*-infected *Anopheles* mosquitoes fed with a high concentration of BrdU in sugar-water. As a result, high frequencies (94 ± 2%) of BrdU$^+$ *Pb* sporozoites were generated, which retained BrdU through its development to the exoerythrocytic forms (EEF) in hepatocytes (Fig. 3 *A*–*C* and *SI Appendix*, Fig. S3*B*). Of note, we switched to using *Pb* in this experiment, because *Py*-infected mosquitoes reared on BrdU-laced water consistently failed to yield sufficient viable sporozoites. We were able to coimmunoprecipitate BrdU and AIM2 from BrdU$^+$*Pb* sporozoite-infected primary mouse hepatocytes, indicating that *Plasmodium* DNA likely directly associated with AIM2 in the infected host cells (Fig. 3*D*). Hepatocytes coincubated with wild-type *Pb* (BrdU$^-$) sporozoites or salivary gland debris extracted from uninfected mosquitoes fed BrdU-laced water served as additional controls in this experiment (*SI Appendix*, Fig. S3*A* and Fig. 3*D*). The above finding was further supported by the observation of colocalization of AIM2 and BrdU$^+$*Pb* EEFs in the infected mouse hepatocytes (Fig. 3*E*).

Although the deficiency of NLRP3 itself did not significantly hamper the control of *Plasmodium* infection in the liver (Fig. 2*C*), NLRP3 is known to cooperate with AIM2 in the control of a variety of intracellular pathogens (45–48). To determine the extent to which NLRP3 receptors might facilitate AIM2-mediated control of *Plasmodium* infection in the liver (or vice versa), we generated a strain of mouse deficient in both AIM2 and NLRP3 (AIM2-NLRP3dKO). Indeed, the deficiency of both receptors impaired the control of *Plasmodium* infection in the liver, significantly more so than when either receptor was independently absent (*SI Appendix*, Fig. S3*C*). It is noteworthy that AIM2, NLRP3, or ASC colocalize with Caspase-1, adjacent to *Plasmodium* in the infected hepatocytes (*SI Appendix*, Fig. S3*D*). This is reminiscent of supramolecular organizing centers formed on membrane-bound organelles within the cytoplasm, which serve as signal amplification platforms to drive Caspase-1-mediated pyroptotic cell-death (49).

While type I IFNs are known to facilitate the control of *Plasmodium* infection in the liver, the exact mechanism behind this process has remained unresolved (8, 12, 14). We observed that *Py* infection enhanced the expression of AIM2 in the infected hepatocytes in a type I IFN-dependent manner (*SI Appendix*, Fig. S4 *A* and *B*). This observation offered a potential pathway through which type I IFNs can facilitate *Plasmodium* control in the liver. Of note, type I IFN stimulation alone was sufficient to enhance AIM2 expression in bone marrow-derived macrophages (BMDMs) as well, strengthening this idea (*SI Appendix*, Fig. S4*C*). Type I IFN treatment has been shown to drive AIM2, ASC, and Caspase-1 transcript levels in THP-1 monocytes (50). Taken together, our data illustrate that the AIM2 receptor in hepatocytes senses *Plasmodium* DNA directly, is induced by type I IFNs, and is instrumental in the innate immune control of malaria in the liver.

Noncanonical Processing of Caspase-1 in Hepatocytes. In the current model of Caspase-1 activation in cells, autoproteolytic

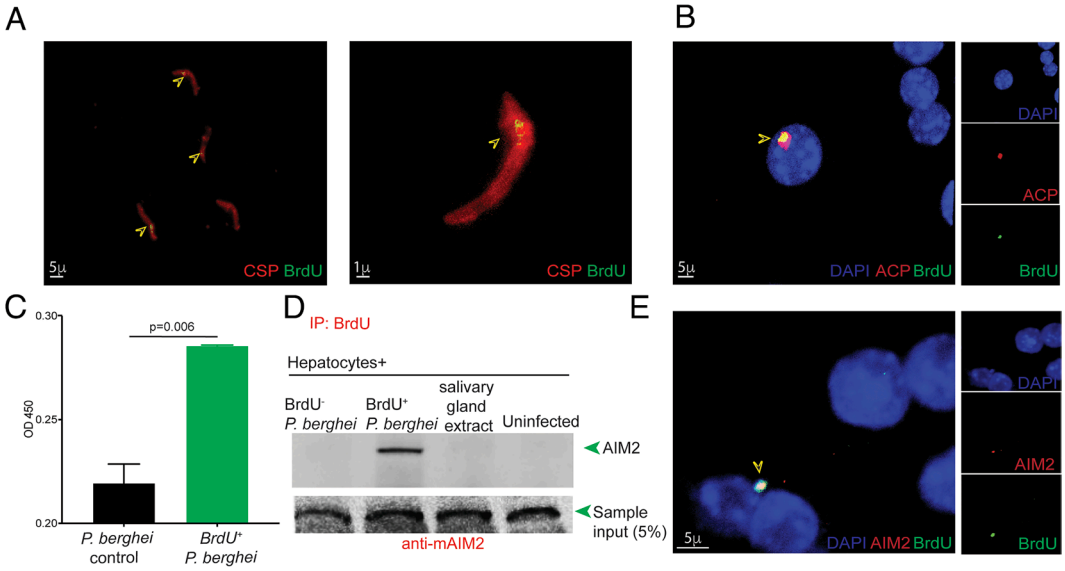

Fig. 3. AIM2 receptor binds *Plasmodium* DNA in the infected hepatocytes. (*A*) Pseudocolored confocal image of a representative field (>10 fields) of BrdU$^+$ *Pb* sporozoite stages (stained using anticircumsporozoite protein, CSP) derived from infected mosquitoes. CSP is located on the plasma membrane of the sporozoites. Arrows indicate BrdU incorporation. Frequency (%) of colocalization of CSP (sporozoites) and BrdU: 94 ± 2.0. Data presented as mean ± SEM from ≥10 microscopy fields obtained from at least 3 separate experiments. (*B*) Representative (>10 fields) pseudocolored confocal image of BrdU$^+$ *Pb* exoerythrocytic form (EEF, stained using anti-Acyl carrier protein, ACP) in an in vitro cultured primary murine hepatocyte at 24 h p.i. ACP-stained *Plasmodium* EEF is indicated by the arrow. Frequency (%) of colocalization of ACP and BrdU in such *Pb*-infected hepatocytes: 91.6 ± 1.42. Data presented as mean ± SEM from ≥10 fields derived from at least 3 separate experiments. (*C*) ELISA comparing lysates of *Pb* sporozoites derived from BrdU-fed or control-infected mosquitoes to determine relative BrdU levels. Data presented as mean ± SEM from 3 technical and two biological replicate experiments, compared with *t* tests to yield the presented *P* value. (*D*) Immunoblot analysis for AIM2 after immunoprecipitation of the whole-cell lysates of primary mouse hepatocytes infected with BrdU$^+$ *Pb* (24 h p.i.), using anti-BrdU antibodies. Hepatocytes were either infected with wild-type *Pb* (BrdU$^-$), coincubated with salivary gland extracts from BrdU-fed mosquitoes, or remained uninfected/untreated to serve as controls. Data represent 4 separate replicate experiments. (*E*) Representative pseudocolored confocal image (>10 fields) of BrdU$^+$ *Pb* exoerythrocytic form in an in vitro cultured primary murine hepatocyte at 24 h p.i. Arrow indicates the developing parasite. Frequency (%) of colocalization of AIM2 and BrdU: 58.50 ± 1.42. Data presented as mean ± SEM from ≥10 fields derived from at least 3 separate experiments.

cleavage of the procaspase-1 (p46) molecule into its constituent CARD, p20, and p10 domains is followed by the formation of catalytically functional hetero-tetramers composed of the p20 (~20 kDa) and p10 (~10 kDa) subunits, which carry out the downstream biological functions of Caspase-1 (26, 27) (*SI Appendix*, Fig. S5*A*). To confirm Caspase-1 activation in the *Plasmodium*-infected hepatocytes biochemically, we infected primary mouse hepatocyte cultures with *Py* sporozoites and examined the presence of Caspase-1 p20 subunit using western blotting. Surprisingly, and in stark contrast to the existing paradigm, we observed that Caspase-1 processing in both murine and human primary hepatocytes infected with *Plasmodium* generated a Caspase-1 cleavage product of approximately 32 kDa (which we call p32), without any detectable p10 or p20 cleavage forms (Fig. 4 *A*–*C* and *SI Appendix*, Fig. S5 *B* and *C*). Treatment of primary hepatocytes with the standard inducers of Caspase-1 activation- LPS and ATP also induced p32, unlike in the case of BMDMs, where the conventionally processed p20 subunit was readily generated (Fig. 4 *A*–*C*). This suggested that the generation of p32 is likely an inherent, hitherto unknown characteristic of Caspase-1 processing in hepatocytes.

To test whether the generation of p32 could be an artifact of in vitro culture or stimulation of hepatocytes, we infected liver-humanized chimeric mice with *Pf* sporozoites in which the *Pf* infection would be limited to the hepatocytes of human origin (51). Only human Caspase-1 p32 was immunoprecipitated from the whole-liver lysates of these mice (Fig. 4*D*), indicating that Caspase-1 is noncanonically processed in the human hepatocytes in vivo following *Plasmodium* infection.

Remarkably, when probed with either p20 or p10 Caspase-1 subunit-specific antibodies separately, only the p32 Caspase-1 was detected in *Py*-infected hepatocytes. This is unlike in the BMDMs stimulated with LPS and ATP, where distinct p20 and p10 cleavage products were clearly detected (Fig. 4*E*). This finding suggested that Caspase-1 p32 observed in hepatocytes may be composed of unseparated p20 and p10 domains of Caspase-1. To objectively test this possibility, we employed a p20 subunit-specific antibody to immunoprecipitate (IP) Caspase-1 cleavage products from the whole-cell lysates of *Py*-infected hepatocytes, resolved it on a denaturing gel, and probed with the p10 subunit-specific antibody. The observation of p32 immunoprecipitate in this experiment confirmed that p32 is indeed composed of unseparated p20 and p10 domains (Fig. 4*F*).

A short-lived (<30 min after inflammasome formation) intermediate product of conventional Caspase-1 processing, composed of unseparated CARD and p20 domains (p33, *SI Appendix*, Fig S5*A*) has been reported in LPS- and ATP-stimulated BMDMs (52). However, Caspase-1 p32 generated in hepatocytes remained consistently detectable for over 24 h post infection unlike the p33 intermediate (*SI Appendix*, Fig. S5*B*).

One potential reason for the generation of p32 in hepatocytes is the existence of alternate spliced form of procaspase-1, where the interdomain linker (IDL) sequence connecting p20 and p10 subunits is not amenable to proteolytic processing (*SI Appendix*, Fig. S5*A*) (26). Therefore, to further characterize p32 and to determine if p32 may be a product of alternate splicing of procaspase-1 in hepatocytes, we sequenced the hepatocyte procaspase-1 transcripts in *Py*-infected or LPS+ATP stimulated primary mouse

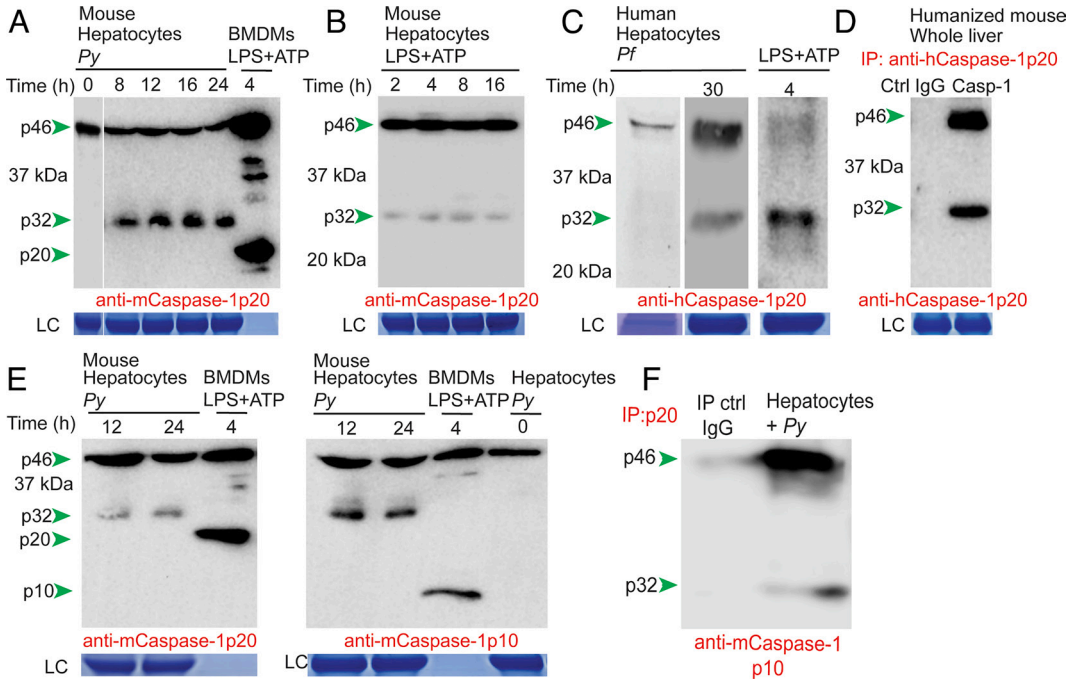

Fig. 4. Non-canonical processing of Caspase-1 in hepatocytes. (*A* and *B*) Immunoblot screen for Caspase-1 cleavage forms in primary mouse hepatocytes infected with *Py* (*A*) or treated with LPS+ATP (*B*) for the indicated time-frames. Murine BMDMs coincubated with LPS+ATP served as control. Caspase-1 p20 subunit-specific antibodies detect uncleaved procaspase-1 (p46) and the cleaved Caspase-1 products, p32 or p20. (*C*) Immunoblot analysis for cleaved Caspase-1 in human hepatocytes infected with *Pf* (*Left*) or treated with LPS+ATP (*Right*) for the indicated time-frames. (*D*) Immunoblot analysis confirming the identity of Caspase-1 pulled down from whole-liver lysates of liver-humanized mice infected with *Pf* (30 h p.i.), using with anti-p20-specific antibody. (*E*) Immunoblot analysis for Caspase-1 cleavage in primary mouse-hepatocytes infected with *Py* and probed with Caspase-1 p20 subunit (*Left*) or Caspase-1 p10 subunit (*Right*)-specific antibodies. Murine BMDMs coincubated with LPS+ATP served as the standard for conventional Caspase-1 cleavage pattern, indicating p20 and p10. (*F*) Immunoblot analysis in whole-cell lysates of primary B6 hepatocytes cocultured with *Py* for 24 h, immunoprecipitated with anti-mCaspase-1p20 and the precipitate probed with anti-mCaspase-1p10. (*A*–*E*) LC represents the protein loading controls from the SDS–PAGE, to provide an estimate of the representation of pro/Caspase-1 in the total protein content of the hepatocytes or BMDMs. Note that these are single exposure blots and due to the high signal intensity, the amount of total protein added from the BMDM lysates was insufficient for detection by Coomassie blue staining in the loading control. All data are representative of at least 3 separate experiments.

hepatocytes. We found that the Caspase-1 sequence in such hepatocytes did not differ from that of myeloid cells and the IDL sequence in the hepatocyte transcript was identical to that of the reference sequence (*SI Appendix*, Fig. S5*D*). In addition, bioinformatic analysis of our (9) and others' (53–56) published RNAseq data also did not indicate the presence of any procaspase-1 splice variants in the infected or uninfected, human or murine hepatocytes.

In order to rule out the possibility that contaminating mosquito debris is an inadvertent contributor to the Caspase-1 activation observed in the above experiments, we compared uninfected or *Py*-infected hepatocytes with hepatocytes coincubated with salivary gland extracts from uninfected mosquitoes (mock infection). Only *Py*-infected hepatocytes exhibited any detectable Caspase-1 processing (*SI Appendix*, Fig. S5*E*). In addition, transfection of *Plasmodium* DNA into primary hepatocytes and BMDMs induced the Caspase-1 activation in an AIM2-dependent manner, corroborating our previous finding that *Plasmodium* DNA can be directly sensed by AIM2 to induce Caspase-1 activation (*SI Appendix*, Fig. S5 *E* and *F*). Together, these observations challenged the universality of the existing model of Caspase-1 processing dynamics, and suggests that Caspase-1 biochemistry may vary based on the cells or tissues involved.

Caspase-1 Controls Liver-Stage Malaria through GSDMD Activation. Proteolytically activated Caspase-1 is known to control intracellular pathogens through the induction programmed cell-death in the host cells, in addition to the induction of proinflammatory cytokine responses (19). Caspase-1 proteolytically activates GSDMD, which generates plasma membrane pores and causes osmotic instability in host cells (28, 57). This process results in the elimination of the pathogen along with its host cell. *Py* infection induced significant cell-death in hepatocytes in an AIM2 and GSDMD-dependent manner (Fig. 5*A*). We observed that the hepatocytes underwent characteristic vacuolation and rupture following *Py* infection in a GSDMD-dependent manner, suggesting that *Py* infection induced pyroptotic cell-death in hepatocytes (Fig. 5*B* and Movies S1 and S2) (58). Caspase-1-dependent proteolytic cleavage of GSDMD was evident in *Py*-infected hepatocytes (Fig. 5*C*). Consistent with these findings, genetic deficiency, or therapeutic inhibition of GSDMD using the drug disulfiram (59) significantly compromised the control of malaria in the liver (Fig. 5 *D* and *E*). These results indicated that AIM2-mediated Caspase-1 activation brings about GSDMD-mediated pyroptotic cell-death and elimination of *Plasmodium*-infected hepatocytes, resulting in a better overall control of malaria in its preerythrocytic stage.

In addition to GSDMD activation, Caspase-1 is also known to mature proinflammatory cytokines such as IL-1 and IL-18 in host cells. Although these cytokines have the ability to support the recruitment of various antigen presenting and phagocytic cells to the site of infection, they appear to have a limited role in the elimination of the intracellular niche of pathogens, or the pathogen itself (57, 60). Compared with the BMDMs, primary mouse hepatocytes produced undetectable levels of mature IL-1β or IL-18 (*SI Appendix*, Fig. S6 *A* and *B*), although the activated Caspase-1 in hepatocytes was catalytically functional (*SI Appendix*, Fig. S6*C*). In support of the above finding, therapeutic blockade of IL-1 signaling did not impact the control of *Py* infection in mouse livers (*SI Appendix*, Fig. S6*D*). These findings further reinforced the premise that programmed cell-death itself may be the principal means of Caspase-1-mediated control of liver-stage malaria. Together, these data suggest that AIM2-mediated Caspase-1 activation in hepatocytes promotes the control of malaria through GSDMD-mediated pyroptotic elimination of infected hepatocytes.

Discussion

Plasmodium parasites have to undergo development in the liver before progressing to the blood-stage of infection (2). Therefore, by arresting *Plasmodium* life-cycle in the liver, clinical malaria and transmission can be completely prevented (3), making the inhibition of *Plasmodium* development in the liver a key priority of the current vaccination and therapeutic strategies against malaria (4, 5). Innate immune responses are instrumental in bringing about rapid and early control of infections before the more mechanistically elaborate adaptive responses can be invoked (16). Considering the very short time-frame of *Plasmodium* development in the liver, innate immune responses elicited in the liver serve a critical function in impeding the progression of *Plasmodium* infection to the blood-stage (12, 14, 61, 62). Several innate immune pathways stimulated by *Plasmodium* during its blood-stage have been identified in the past (14, 48, 63–65). However, natural transmission of malaria occurs only through the inoculation of sporozoites, which have to undergo development in the liver in mammalian hosts before advancing to the blood-stage (2). Furthermore, the innate responses generated against blood-stage malaria are limited to the myeloid cells, and may not be particularly effective in limiting the onset of clinical malaria (14). Innate immune responses that impede *Plasmodium* infection in the liver actively limit the incidence and severity of clinical malaria (7, 12). Therefore, understanding how natural immune responses control *Plasmodium* infection during its preerythrocytic development is critical. Here, we describe a pathway of innate immunity to malaria in which AIM2 sensors in hepatocytes detect *Plasmodium* DNA to induce Caspase-1 activation, aiding the control of malaria in the liver. We also show that proteolytic activation of Caspase-1 occurs in an unconventional manner in hepatocytes, and it enables the control of liver-stage malaria primarily through the induction pyroptotic cell-death.

In order to gain a comprehensive and unbiased view of the transcriptional changes produced by *Plasmodium* infection in hepatocytes, we performed scRNA sequencing of primary human hepatocytes infected with *Pf*. As discussed in the results section, utilizing primary hepatocytes and a field isolate of *Pf* in this experiment allowed us to create a valuable resource that, as close as practically possible, would represent the changes induced in the hepatocytes of human malaria patients. The transcriptional upregulation of genes pertinent to hepatocyte injury, inflammation, and cell-death pathways suggested that *Plasmodium* infection is a potential driver of the inflammasome pathway in hepatocytes. It is known that PAMP stimulation can transcriptionally upregulate certain PRRs and proinflammatory cytokine genes in hepatocytes (37). Our experimental data eventually validated the above speculations with the observation of Caspase-1 activation and pyroptotic cell-death in *Plasmodium*-infected hepatocytes. Of note, the pyroptotic cell-death responses associated with *Plasmodium* infection in hepatocytes has been considered a critical driver of the adaptive immune responses generated against liver-stage malaria (9). Our transcriptional data also showed that a variety of metabolic and molecular synthetic pathways are impacted in the hepatocytes following *Plasmodium* infection. Considering that hepatocytes have a significant role in the breakdown (e.g., toxins) or synthesis (e.g., albumin, cholesterol) of biomolecules, future studies relying on the resource we have generated would provide insights into the biological impact of *Plasmodium* infection on the hepatocytes and the liver as a whole.

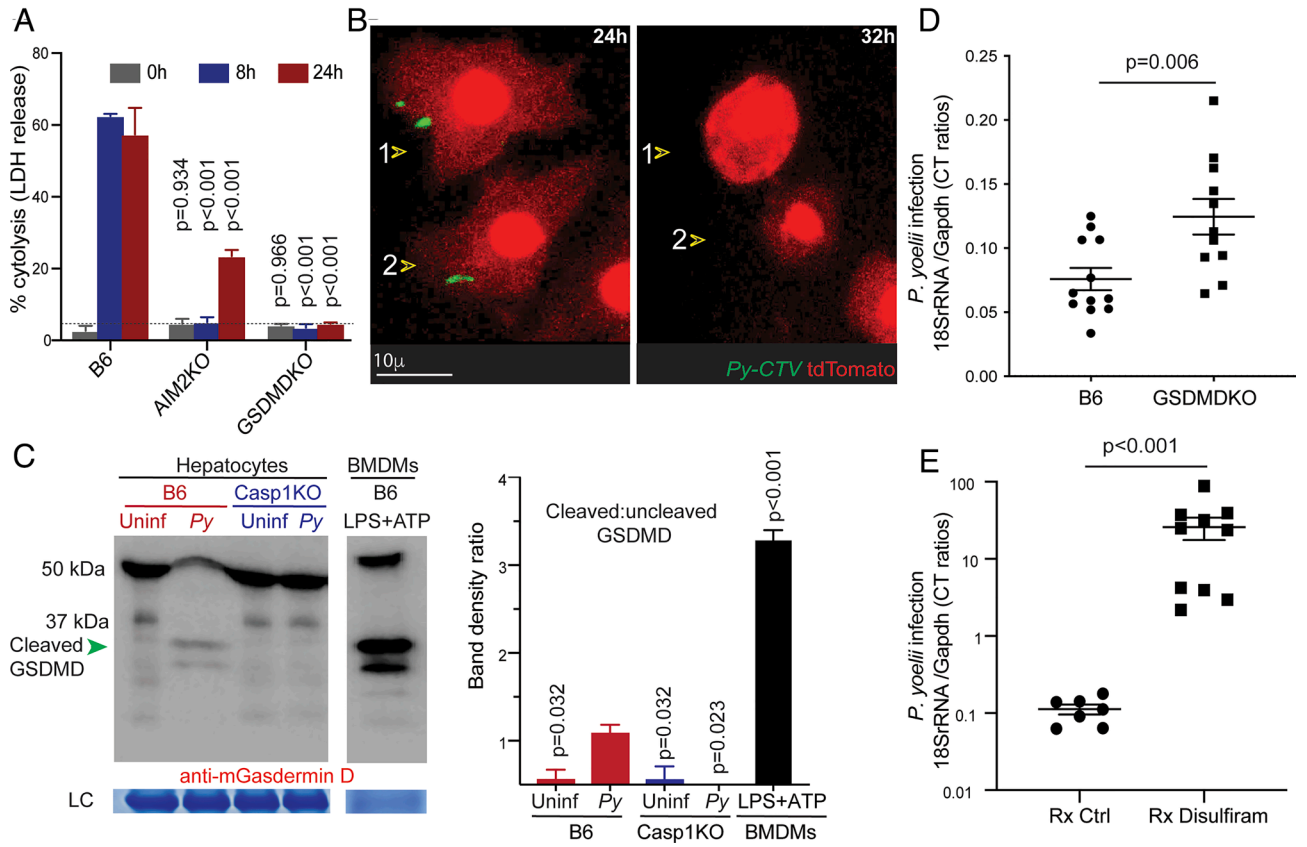

Fig. 5. Caspase-1 activation induces GSDMD-mediated cell-death in hepatocytes. (*A*) Comparison of cytolysis determined by LDH release assay in *ex vivo* cultured primary hepatocytes derived from the indicated mice, coincubated with *Py* for the indicated times. Data presented as mean ± SEM, analyzed using ANOVA with Dunnett's correction comparing each time point to the corresponding one in B6 mice, to yield the presented *P*-values. The dotted line indicates median cytolysis levels in B6 hepatocytes treated for 24 h with salivary gland extracts derived from uninfected mosquitoes. (*B*) Representative confocal time-lapse images showing primary hepatocytes from tdTomato$^+$ B6 mice infected with *Py* (CellTrace Violet$^+$, indicated by arrows), observed at 24 h and 32 h of coincubation. Hepatocyte #1 and #2 shown on left just prior to undergoing pyroptotic rupture; please see Movie S1 for the full sequence of events. (*C*) Immunoblot analysis for GSDMD cleavage in primary hepatocytes obtained from the indicated mice coincubated with *Py,* at 24 h. BMDMs treated with LPS+ATP (4 h) served as the positive control. LC: loading control. Bar graphs on the right depict the relative densities of cleaved GSDMD, presented as the mean ratio of cleaved: uncleaved GSDMD bands calculated from three separate immunoblots. Data presented as mean ± SEM, analyzed using ANOVA comparing each group to the B6 *Py* group to yield the presented *P*-values. (*A–C*): all data shown represent ≥3 separate experiments. (*D*) Scatter plots showing relative liver-parasite burdens in the indicated mice inoculated with *Py,* 36 h p.i. (*E*) Scatter plots showing relative liver-parasite burdens in the vehicle-treated (Rx ctrl) or Disulfiram-treated (−1 d, 0, 1 d p.i) mice inoculated with *Py,* 42 h p.i. (*D* and *E*) Data presented as mean ± SEM, analyzed with 2-tailed *t* tests to yield the presented *P* value and combined from three separate replicate experiments.

Immune responses to *Plasmodium* infection in the liver remain relatively understudied despite its immense translational relevance to the treatment and prevention of malaria (4, 5). Recognition of a functional AIM2-Caspase-1 axis in the *Plasmodium*-infected hepatocytes offers opportunities to therapeutically and immunologically improve antimalarial immunity (66). For instance, enhancing innate immune responses by employing exogenous PAMPs is known to engender better adaptive responses in the context of live-vaccines (67). Although type I IFNs produced by *Plasmodium*-infected hepatocytes facilitate innate control of liver-stage malaria (8, 10, 12), how type I IFNs exert control of malaria in the liver has not been fully characterized. We show that type I IFNs enhance AIM2 expression in hepatocytes. This would enhance the sensitivity of hepatocytes to *Plasmodium* DNA. Efficient sensing of *Plasmodium* DNA by infected hepatocytes would lead to the rapid elimination of such hepatocytes by pyroptosis, thereby limiting *Plasmodium* infection in the liver. Although we present evidence for the association of *Plasmodium* DNA with host AIM2 receptors, there is a possibility of host's own DNA, including mitochondrial DNA triggering the AIM2-mediated inflammasome pathway in hepatocytes (68). Only future studies will shed light into such prospects.

In addition to AIM2 or NLRP3, host or pathogen-derived DNA that gains access to host cell cytosol can be detected by a variety of other sensors such as STING, IFI16/p204, etc. (69). Several factors such as the expression levels of DNA sensors, various partner molecules in the sensing pathway, etc. would impact the relevance of such sensors in mediating protection from intracellular pathogens. For instance, we observed that the cGAS/STING pathway does not have a direct role in controlling *Plasmodium* infection in the mouse liver, possibly because hepatocytes do not express significant levels of the STING receptor (12, 70). We have shown previously that type I IFN signaling in hepatocytes help control *Plasmodium* infection in the liver, possibly through the induction of cell-autonomous immune responses (12). We anticipate such responses to target and lyse the intracellular *Plasmodium,* potentially exposing *Plasmodium* nucleic acids to the hepatocyte cytoplasm (8). Only future studies will elucidate the mechanisms by which *Plasmodium*-derived nucleic acids are exposed to the hepatocyte cytosol, or how the hepatocytes respond to the presence of such molecules in the hepatocyte cytoplasm in the context of liver-stage malaria.

Of note, there are conflicting reports about the ability of *Plasmodium* to incorporate BrdU into its genome. It has been

suggested that BrdU may not be incorporated into the DNA of replicating in vitro cultured schizont stage (i.e., during schizogony) of *Pf*, perhaps due to the absence of active thymidine kinase in the parasites in that stage (71). BrdU was not detected using ELISA in *Pf* when cultured in vitro, in the presence of 1 mM BrdU. However, other studies have indicated that *Pf* does incorporate BrdU when cultured in the presence of BrdU, with this approach being adapted for drug discovery efforts (43, 44). We show that BrdU is incorporated by the mouse malaria parasite, *Pb* during its in vivo development in mosquitoes (i.e., during oocyst development), by relying on microscopy and ELISA. We presume that thymidine kinase or a functional ortholog may be conserved and active in the oocyst stage of *Pb*. Only future studies will resolve the differences in BrdU incorporation into various *Plasmodium* species and stages.

Although various groups have examined Caspase-1 activation in the liver in the past, the majority of such studies were conducted using whole-liver extracts that also contained myeloid cells (72, 73), or in neoplastic cell-lines possessing dysregulated cell-death pathways (74–77). In those instances where primary hepatocytes were discretely examined in the context of infectious or aseptic liver diseases, conventionally cleaved Caspase-1 products have consistently remained elusive in the hepatocytes (78–80). We considered the possibility that procaspase-1 expressed in hepatocytes is a splice variant incapable of cleavage at the IDL sequence (*SI Appendix*, Fig. S5*A*). A procaspase-1 variant transgenically generated in *in vitro* cultured BMDMs through site-directed mutagenesis of the autoproteolytic cleavage site in IDL produced unseparated p20 and p10 fragments, akin to p32, and exhibited detectable biological activity (26). Nevertheless, no alternately spliced variants of procaspase-1 were observed in primary human or mouse hepatocytes upon analysis of published transcripts, or by sequencing murine hepatocyte transcripts, suggesting that Caspase-1 p32 generation in hepatocytes is unlikely to be a consequence of modified IDL sequence of procaspase-1 in hepatocytes. Only future studies will determine why procaspase-1 undergoes incomplete processing in the hepatocytes.

Various unconventionally cleaved Caspase-1 products have been reported in other parenchymal cell lineages such as the epithelial cells and neurons, as well as in certain types of neoplasms (81–87). Despite being genetically conserved, Caspase-1 processing is known to generate versatile cleavage products in lower order animals or birds (60). Although Caspase-1 cleavage patterns have evolved to extend the biological functions of Caspase-1 in higher order animals such as mammals, remarkably, Caspase-1 appears to have conserved its ability to induce host cell-death throughout this evolutionary process (60). This suggests that the primary immunological function of Caspase-1 in higher order mammals may be the induction of host cell-death, with the production of proinflammatory responses being a secondary, specialized function present primarily in the more dedicated immune cells. Of note, when Caspase-1 processing was transgenically limited to the p32 form in BMDMs by mutating the IDL sequence of procaspase-1 as described above, such BMDMs generated significantly reduced levels of mature IL-1β in response to *Salmonella* infection or LPS+ATP stimulation, but conserved the ability to undergo cell-death (26). Of note, hepatocyte p32 is catalytically active. It has also been shown that Caspase-mediated cell-death in hepatocytes is crucial to deliver *Plasmodium* antigens to APCs recruited to the infected liver, implying that Caspase-1 function in hepatocytes is vital for the induction of adaptive immune responses against liver-stage malaria (9).

The precedent of undertaking biochemical and functional characterizations of the inflammasome pathway using immune cells and cell-lines may have skewed our understanding of Caspase-1 biology, and may have led to the presumption that Caspase-1 activation and functions are uniform in all cell-types (19, 21, 25, 31). Similarly, usage of cancer cell lines such as hepatoma cells to study *Plasmodium* infection biology may have allowed at least some innate immune pathways pertinent to liver-stage malaria infections to remain elusive. We believe that our focus on purified primary human and mouse hepatocytes have played a crucial role in uncovering AIM2-mediated innate immune response in *Plasmodium* infection in the liver, and of unconventional Caspase-1 processing in hepatocytes. In addition to inspiring future studies that investigate potential immune mechanisms that evoke the release of *Plasmodium* DNA into the host hepatocytes, we believe that this work will invoke fundamental questions about the determinants of unconventional processing of Caspase-1 in hepatocytes, and possibly in other parenchymal cells.

Materials and Methods

Mice and Pathogens. C57BL/6 (B6) mice were purchased from the National Cancer Institute or Jackson Laboratory and liver-humanized mice were obtained from Yecuris. GSDMDKO mice were provided by Dr. Thirumala-Devi Kanneganti (St Jude's Children's Research Hospital), tdTomato expressing mice by Dr. John Englehardt (University of Iowa), ASCKO, NLRP3KO, NLRC4KO, and Casp1/11KO mice by Dr. Fayyaz Sutterwala (Cedar-Sinai), IFNAR1KO, NLRP1bKO, and AIM2KO mice procured from the Jackson laboratory. All mice were housed with appropriate biosafety containment at the animal care units. The animals were treated and handled in accordance with guidelines established by the respective Institutional Animal Care and Use Committees. *Anopheles stephensi* mosquitos parasitized with *P. yoelii* 17XNL (*Py*) and GFP$^+$ *P. yoelii* 17XNL (*Py-GFP*) were obtained from New York University. *A. stephensi* mosquitos infected with *Pf* NF54 or BD007 isolates were obtained from Johns Hopkins University or the University of Georgia. *A. stephensi* mosquitos infected with *P. berghei ANKA* (*Pb*) was obtained from the University of Georgia.

Primary Hepatocyte Culture, In Vitro Sporozoite Infection and PRR Stimulation. Primary hepatocytes were isolated from mice as described in detail before (9). Primary human hepatocyte infection in this study followed published methods (88). The methodological details are described in detail in *SI Appendix*.

scRNAseq and Analysis. Primary human hepatocytes cultured in vivo in replicates were infected with *Pf* (BD007 isolate) and the hepatocytes were analyzed using scRNA sequencing. The methodological details of the experiment and data analysis are described in detail in the *SI Appendix*.

***Plasmodium* Inoculations into Mice.** For sporozoite challenge experiments to determine liver-parasite loads, salivary glands of parasitized *A. stephensi* mosquitoes were dissected and sporozoites were isolated, counted, and injected 3 to 5 × 10^4 in 200 μL RPMI with 1% mouse serum (Innov-research) retroorbitally or into the tail vein of mice (9). For some imaging experiments, parasitized *A. stephensi* mosquitoes (~100/carton) were allowed to bite the abdomen of ketamine anesthetized mice (5/carton) for 6 separate 5-min intervals.

For infecting of liver-humanized mice, *A. stephensi* infected with *Pf* NF54 strain were allowed to bite ketamine-anesthetized liver-humanized mice for 15 min. The remaining sporozoites were subsequently isolated from the same mosquitoes and inoculated intravenously into the tail vein of the mosquito-fed mouse at 7.5 × 10^5 sporozoites per mouse. The animals were euthanized at 30 h p.i. to collect the liver.

Flow Cytometry. Hepatocyte fractions collected after prefusion, density gradient separation, and adhesion to culture plates (dislodged by trypsin, 0.25% trypsin-EDTA, 5 min at 37 °C) were stained with 0.5 μg/mL anti-CD45 F4/80, CD11c, CD11b. or CSF1R (Biolegend) (20 min at 4 °C) to determine the presence of hematopoietic or Kupffer cells, or to phenotypically characterize them as presented in detail before (9). Cells were stained for cell surface markers with appropriate antibodies in PBS for 30 min prior to washing and resuspending in PBS to analyze by flow cytometry. To determine Caspase-1 activation, *Plasmodium*-infected hepatocytes were

tested using the FAM-FLICA Caspase-1 assay kit (ImmunoChemistry Technologies) as per the manufacturer's protocol. Data were acquired on an LSR Fortessa (BD Biosciences) and analyzed with Flowjo (Treestar).

Macrophage Differentiation. BMDMs were prepared as described previously (89). In short, bone marrow cells were grown in L-cell-conditioned IMDM medium (ThermoFisher) supplemented with 10% FCS, 1% nonessential amino acids and 1% penicillin–streptomycin for 5 d to differentiate into macrophages. On day 5, BMDMs were seeded in 6-well cell culture plates. The next day BMDMs were stimulated with 100 ng/mL LPS (3.5 h) followed by 5 mM ATP or 10 μM Nigericin (0.5 h), and the whole-cell lysates or supernatants were collected as indicated.

Assessment of Liver Parasite Burden. Liver parasite burden was assessed by quantitative real-time RT-PCR for parasite 18s rRNA in the livers of mice challenged with sporozoites isolated from infected mosquitoes, as described in detail before (9, 90). RNA was extracted at the indicated time points after *Plasmodium* inoculation using TRIzol, followed by DNase digestion/cleanup using the RNA Clean and Concentrator kit (Zymo Research). 2 μg liver RNA per sample was used for qRT-PCR analysis for *Plasmodium* 18S rRNA using TaqMan Fast Virus 1-Step Master Mix (Applied Biosystems). Data were normalized for input to the GAPDH control (hepatocytes) for each sample and are presented as ratios of *Plasmodium* 18s rRNA to GAPDH RNA. The ratios depict relative parasite loads within an experiment and do not represent absolute values.

BrdU Incorporation. To generate BrdU (5-bromo-2′-deoxyuridine) incorporated sporozoites, female B6 mice were inoculated with *Pb*-infected RBCs (1.5 to 2 × 10^6/ mouse), i.p., followed by mosquito feeding at days 4 and 5 postinfection. The infected mice were anesthetized and exposed to cages containing around 200 overnight-fasted female *A. stephensi* mosquitoes. The mosquitoes were then maintained on 12.5% (w/v) sucrose with 1 mg/mL BrdU, at 19 to 20 °C and 80% relative humidity. The sucrose-BrdU solution was made fresh and replaced every 2 d, until the mosquitoes were dissected to obtain the sporozoites on day 21 after the initial feeding. To incorporate BrdU into DNA of B16 melanoma cells, BrdU (10 μM) was added to the tissue culture media and cultures maintained for 7 d. To prepare salivary gland extracts from BrdU-fed mosquitoes, we maintained the uninfected mosquitoes on sucrose-BrdU solution as described above. Their salivary glands were removed and processed as for sporozoite extraction. The salivary gland extracts from BrdU-fed *Pb*-infected or uninfected mosquitoes were diluted to equivalent amounts for immunoprecipitation or flow-cytometry assays.

Cell-Death Assay. Lactate dehydrogenase (LDH) release assay to determine cell lysis: Overnight cultures of 5 × 10^4 hepatocytes/ well in 48-well plates were inoculated with 2.5 × 10^4 *Py* sporozoites. Cell culture supernatants were replaced with fresh media at 4 h incubation after washing the cells twice with media, to remove free sporozoites. Culture supernatant was subsequently collected at various time points and assayed for LDH as a measure of total cytolysis, using the CytoTox 96 Non-Radioactive Cytotoxicity Assay (Promega) according to the manufacturer's instructions. %Cytolysis calculated as 100× (experimental LDH release signal/ maximum LDH release signal).

Microscopy. Liver sections (30 μM thickness) collected from infected (5 × 10^5 *Py* or 7.25 × 10^5 *Pf* sporozoites) mice were fixed, permeabilized with 1% Triton X-100 (Fisher Bioscience) and imaged after staining. In addition, cultured hepatocytes in 10u-slide for chemotaxis (ibidi) were imaged live. Images were acquired on SP8 NLO Microscope (Leica) using a 10×/0.40 dry objective (live) or 25×/0.95 water immersion objective with coverslip correction (fixed), as described in detail previously (91). All images acquired were processed using Imaris software (Bitplane).

Caspase-1 (p10, polyclonal, Bioss Antibodies) was used on human hepatocytes and 1 μg/mL Caspase-1 (p20, Clone Casper-1, Adipogen), 0.5 μg/mL GasderminD (Clone EPR19828, AbCam), 0.5 μg/mL ASC (Clone D2W8U, Cell Signaling), 0.5 μg/mL NLRP3 (Clone 768319, R&D), or 0.5 μg/mL AIM2 (Clone EPR18793, AbCam) on mouse hepatocytes. Pfhsp70 (polyclonal, GenWay) was used to mark *Pf*. The following were used to identify *Py*: hep17 (gift from Dr. Scott Lindner, Pennsylvania State University), ACP or CSP (polyclonal, 1:100, gifts from Dr. Stefan Kappe, Seattle Children's Hospital), along with 0.4 μg/mL anti-BrdU (clone BU1/75, ThermoFisher) or 5 μM CellTrace Violet (CTV, ThermoFisher). The following were used to identify *Pb*: GFP (Clone FM264G) and UIS4 (polyclonal, 1:100, gift from Dr. Scott Lindner, Pennsylvania State University). For live imaging, hepatocytes were cultured overnight in collagen coated chamber slides (ibidi) and infected with *Plasmodium*. Cultures were maintained in a climate-controlled chamber during imaging. For determining BrdU incorporation in *Plasmodium*, air-dried sporozoites (10^4/well) in "PTFE" printed slides (Electron Microscopy Sciences), or frozen sections from infected livers were used. Samples were fixed with 4% paraformaldehyde/PBS (10 min), permeabilized with Cytofix/Cytoperm buffer (BD Biosciences) for 15 min/4 °C or 1% tritonX100, washed once with Perm/Wash buffer (BD Biosciences), treated with Cytoperm Permeabilization Buffer Plus (BD Biosciences), for 15 min/4 °C, washed again with Perm/Wash buffer, and treated again with Cytofix/Cytoperm (BD Biosciences) for 15 min/4 °C. After washing with Perm/Wash buffer again, the samples were treated with DNAse in PBS/BSA for 90 min at 37 °C. The samples were subsequently washed with Perm/Wash buffer and coincubated with rat monoclonal anti-BrdU antibody (Clone BU-1, Thermofisher) and anti-CSP (sporozoites) or anti-ACP (schizont) antibodies. Subsequently the samples were washed thrice with Perm/Wash buffer, probed with 5 μg/mL fluorophore-conjugated secondary antibodies and 0.1 μg/mL of DAPI, washed thrice with Perm/Wash buffer, and imaged.

The percentage of *Plasmodium*-infected hepatocytes in which specific subcellular components were detected (e.g., Caspase-1) was represented by its 'frequency of association', and the percentage of *Plasmodium*-infected hepatocytes in which distinct subcellular components colocalized with each other spatially (e.g., *Plasmodium* and AIM2) was represented by 'frequency of colocalization'. Data are presented in the corresponding figure legends as mean ± SEM.

Transfection of Cells. Hepatocytes (7 × 10^5 cells) were transfected with various nucleic acids (at 6 μM concentration) using the Mouse/ Rat hepatocyte Nucleofector kit (Lonza) following the manufacturer's protocol. The transfected cells were transferred to collagen-coated wells, 16 h prior to infection or treatments.

Differentiated BMDMs were detached by treatment with trypsin and resuspended at a concentration of 10^6 cells per 100 μL of nucleofector solution. These cells were transfected with ON-TARGETplus SMARTpool siRNAs (Dharmacon) using the Mouse Macrophage Nucleofector kit (Amaxa) following the manufacturer's protocol. The transfected cells were transferred to plates and allowed to recover for 24 to 48 h prior to infections or treatments. The DNA extracted from *Plasmodium* or B16 tumor cells lines using Phenol/chloroform/isoamyl alcohol precipitation was sonicated at 20% power (Qsonica) with 5 s/45 s on/off cycle, 8 times, to shear it to uniform 200-bp fragments. BMDMs in 6-well plates were transfected using lipofectamine2000 as described before (92).

Therapeutic Regimens. The following treatment regimens were used in this study: siRNA (corresponding Dharmacon siGENOMESMARTpool): 1 nM/mouse, hydrodynamic i.v., −1 or −2 dpi, Poly I:C (Invivogen): 100 μg/mouse, hydrodynamic i.v., Mammalian expression plasmids: 10 μg/ mouse, Anakinra: 10 mg/kg, i.v., −1,0,1 dpi, Disulfiram (Sigma-Aldrich): 50 mg/kg in sesame oil, i.p.

Hydrodynamic Delivery of Nucleic Acids. Hydrodynamic injections were performed as described in detail before (93). In short, the desired amount of the siRNA was resuspended in PBS (at 10% volume/ body weight of the mouse) and delivered to the tail vein of mice, using constant pressure, within 7 s. The mice were then placed on a warm heating pad and allowed to recover for about 30 min, before being transferred back into their cages.

Inflammasome Activity Assay. Caspase-1 activity was assayed in cells as described in detail before (94). In short, 8 × 10^5 hepatocytes from 24 h infected or uninfected cultures were lysed and the supernatants were assayed for residual Caspase-1 activity by its ability to cleave the fluorogenic substrate Z-YVAD-AFC (Enzo) by incubating at 37 °C for 60 min. The fluorescence was evaluated at Ex/Em 400/505 in a microplate reader (SynergyH1, BioTek).

ELISA. To determine BrdU incorporation in sporozoites, ELISA was performed as described in detail before (71). The details are described in the *SI Appendix*.

Western Blot and Immunoprecipitation Assays. Western blots were performed as detailed before (89). Immunoprecipitation was carried out as described before (95). The details of these processes are described in the *SI Appendix*.

Sequencing. To determine the sequence of procaspase-1 transcripts in hepatocytes, total RNA was prepared as from the hepatocytes as described above; cDNA

was synthesized as described in detail before (96), and the procaspase-1 gene was amplified with the following primers: 5′-atggctgacaagatcctgagggcaaag-3′ (F) and 5′-ttaatgtcccgggaagaggtagaaac-3′ (R). The amplicons were cloned using TOPO TA cloning kit (Invitrogen) following the manufacturer's protocol and multiple clones (>20) sequenced.

Statistical Analyses. Data were analyzed using Prism7 software (GraphPad) and as indicated in figure legends. The exact P values are indicated in the figures, except when <0.001. In the case of latter, we show it as $p < 0.001$.

Data, Materials, and Software Availability. Primary RNA sequencing data are deposited with NCBI and is available from *BioProject* PRJNA694978. The other data supporting the findings of this study are available within the article or the *SI Appendix* files.

ACKNOWLEDGMENTS. We thank Dr. Rick Tarleton for comments, Gibran Nasir for preparing humanized mice for analyses, Dr. Magdy Alabady for assistance with scRNAseq, Dr. Teneema Kuriakose for helpful discussions, Carson Bowers for help with the mouse colonies, and Dr. Fayyaz Sutterwala for providing valuable knock-out mice. We also express our gratitude to the UGA CTEGD Flow Cytometry Core, UI Central Microscopy Research facility, UGA CTEGD Sporocore, UGA Georgia Genomics and Bioinformatics Core, Iowa Institute of Human Genetics, UGA and UIowa animal research facility staff and the NYU and Johns Hopkins Malaria Institute Insectary Cores. Support for these studies was provided by NIH (AI168307 to S.P.K., AI85515, AI95178, AI100527 to J.T.H., AI132359 to P.S. and K22AI127836 to P.G.) and the UGA Research Foundation (Startup funding to S.P.K.).

Author affiliations: [a]Department of Cellular Biology, University of Georgia, Athens, GA 30605; [b]Center for Tropical and Emerging Global Diseases, University of Georgia, Athens, GA 30605; [c]Department of Internal Medicine, University of Iowa, Iowa City, IA 52242; [d]Institute of Bioinformatics, University of Georgia, Athens, GA 30605; [e]Department of Pathology, University of Iowa, Iowa City, IA 52242; [f]Department of Infectious Diseases, University of Georgia, Athens, GA 30605; [g]Johns Hopkins Malaria Research Institute, Johns Hopkins University, Baltimore, MD 21205; [h]Department of Molecular Microbiology and Immunology, Johns Hopkins University, Baltimore, MD 21205; [i]Department of Immunology, St. Jude Children's Research Hospital, Memphis, TN 38105; and [j]Interdisciplinary Graduate Program in Immunology, University of Iowa, Iowa City, IA 52242

1. WHO, World Malaria Report 2019 (World Health Organization, 2019), citeulike-article-id:13565866.
2. A. F. Cowman, J. Healer, D. Marapana, K. Marsh, Malaria: Biology and disease. *Cell* **167**, 610–624 (2016).
3. C. Marques-da-Silva, K. Peissig, S. P. Kurup, Pre-erythrocytic vaccines against malaria. *Vaccines (Basel)* **8**, 400 (2020).
4. A. X. Mo, G. McGugan, Understanding the liver-stage biology of malaria parasites: Insights to enable and accelerate the development of a highly efficacious vaccine. *Am. J. Trop. Med. Hyg.* **99**, 827–832 (2018).
5. A. X. Y. Mo *et al.*, Understanding vaccine-elicited protective immunity against pre-erythrocytic stage malaria in endemic regions. *Vaccine* **38**, 7569–7577 (2020).
6. Y. Antonova-Koch *et al.*, Open-source discovery of chemical leads for next-generation chemoprotective antimalarials. *Science* **362**, eaat9446 (2018).
7. X. He, L. Xia, K. C. Tumas, J. Wu, X. Z. Su, Type I interferons and malaria: A double-edge sword against a complex parasitic disease. *Front. Cell Infect. Microbiol.* **10**, 594621 (2020).
8. P. Liehl *et al.*, Host-cell sensors for Plasmodium activate innate immunity against liver-stage infection. *Nat. Med.* **20**, 47–53 (2014).
9. S. P. Kurup *et al.*, Monocyte-derived CD11c(+) cells acquire plasmodium from hepatocytes to prime CD8 T cell immunity to liver-stage malaria. *Cell Host Microbe.* **25**, 565–577.e566 (2019).
10. J. L. Miller, B. K. Sack, M. Baldwin, A. M. Vaughan, S. H. Kappe, Interferon-mediated innate immune responses against malaria parasite liver stages. *Cell Rep.* **7**, 436–447 (2014).
11. E. Real *et al.*, Plasmodium UIS3 sequesters host LC3 to avoid elimination by autophagy in hepatocytes. *Nat. Microbiol.* **3**, 17–25 (2018).
12. C. Marques-da-Silva *et al.*, Direct type I interferon signaling in hepatocytes controls malaria. *Cell Rep.* **40**, 111098 (2022).
13. R. E. Howes *et al.*, Global epidemiology of Plasmodium vivax. *Am. J. Trop. Med. Hyg.* **95**, 15–34 (2016).
14. R. T. Gazzinelli, P. Kalantari, K. A. Fitzgerald, D. T. Golenbock, Innate sensing of malaria parasites. *Nat. Rev. Immunol.* **14**, 744–757 (2014).
15. H. Kumar, T. Kawai, S. Akira, Pathogen recognition by the innate immune system. *Int. Rev. Immunol.* **30**, 16–34 (2011).
16. A. Iwasaki, R. Medzhitov, Control of adaptive immunity by the innate immune system. *Nat. Immunol.* **16**, 343–353 (2015).
17. S. N. Kariuki, T. N. Williams, Human genetics and malaria resistance. *Hum. Genet.* **139**, 801–811 (2020).
18. A. V. Hill, Malaria resistance genes: A natural selection. *Trans. R. Soc. Trop. Med. Hyg.* **86**, 225–226, 232 (1992).
19. P. Broz, V. M. Dixit, Inflammasomes: Mechanism of assembly, regulation and signalling. *Nat. Rev. Immunol.* **16**, 407–420 (2016).
20. J. von Moltke, J. S. Ayres, E. M. Kofoed, J. Chavarria-Smith, R. E. Vance, Recognition of bacteria by inflammasomes. *Annu. Rev. Immunol.* **31**, 73–106 (2013).
21. P. Broz, Recognition of intracellular bacteria by inflammasomes. *Microbiol. Spectr.* **7**, 1–11 (2019).
22. D. S. Zamboni, D. S. Lima-Junior, Inflammasomes in host response to protozoan parasites. *Immunol. Rev.* **265**, 156–171 (2015).
23. A. H. Tavares, P. H. Burgel, A. L. Bocca, Turning up the heat: Inflammasome activation by fungal pathogens. *PLoS Pathog.* **11**, e1004948 (2015).
24. B. Briard *et al.*, Fungal ligands released by innate immune effectors promote inflammasome activation during Aspergillus fumigatus infection. *Nat. Microbiol.* **4**, 316–327 (2019).
25. D. Sharma, T. D. Kanneganti, The cell biology of inflammasomes: Mechanisms of inflammasome activation and regulation. *J. Cell Biol.* **213**, 617–629 (2016).
26. P. Broz, J. von Moltke, J. W. Jones, R. E. Vance, D. M. Monack, Differential requirement for Caspase-1 autoproteolysis in pathogen-induced cell death and cytokine processing. *Cell Host. Microbe.* **8**, 471–483 (2010).
27. H. Guo, J. B. Callaway, J. P. Ting, Inflammasomes: Mechanism of action, role in disease, and therapeutics. *Nat. Med.* **21**, 677–687 (2015).
28. J. Shi, W. Gao, F. Shao, Pyroptosis: Gasdermin-mediated programmed necrotic cell death. *Trends Biochem. Sci.* **42**, 245–254 (2017).
29. J. Shi *et al.*, Cleavage of GSDMD by inflammatory caspases determines pyroptotic cell death. *Nature* **526**, 660–665 (2015).
30. X. Liu *et al.*, Inflammasome-activated gasdermin D causes pyroptosis by forming membrane pores. *Nature* **535**, 153–158 (2016).
31. D. Zheng, T. Liwinski, E. Elinav, Inflammasome activation and regulation: Toward a better understanding of complex mechanisms. *Cell Discov.* **6**, 36 (2020).
32. A. S. Yazdi, S. K. Drexler, J. Tschopp, The role of the inflammasome in nonmyeloid cells. *J. Clin. Immunol.* **30**, 623–627 (2010).
33. P. Kuri *et al.*, Dynamics of in vivo ASC speck formation. *J. Cell Biol.* **216**, 2891–2909 (2017).
34. A. L. Fridman, M. A. Tainsky, Critical pathways in cellular senescence and immortalization revealed by gene expression profiling. *Oncogene* **27**, 5975–5987 (2008).
35. C. Wang, M. P. Lisanti, D. J. Liao, Reviewing once more the c-myc and Ras collaboration: Converging at the cyclin D1-CDK4 complex and challenging basic concepts of cancer biology. *Cell Cycle* **10**, 57–67 (2011).
36. X. Liu *et al.*, There are only four basic modes of cell death, although there are many ad-hoc variants adapted to different situations. *Cell Biosci.* **8**, 6 (2018).
37. S. Gaul *et al.*, Hepatocyte pyroptosis and release of inflammasome particles induce stellate cell activation and liver fibrosis. *J. Hepatol.* **74**, 156–167 (2021).
38. T. Fernandes-Alnemri *et al.*, The AIM2 inflammasome is critical for innate immunity to Francisella tularensis. *Nat. Immunol.* **11**, 385–393 (2010).
39. S. E. Warren *et al.*, Cutting edge: Cytosolic bacterial DNA activates the inflammasome via Aim2. *J. Immunol.* **185**, 818–821 (2010).
40. Y. Fu, Y. Ding, T. L. Zhou, Q. Y. Ou, W. Y. Xu, Comparative histopathology of mice infected with the 17XL and 17XNL strains of Plasmodium yoelii. *J. Parasitol.* **98**, 310–315 (2012).
41. N. Kayagaki *et al.*, Non-canonical inflammasome activation targets caspase-11. *Nature* **479**, 117–121 (2011).
42. A. J. Radtke *et al.*, Lymph-node resident CD8alpha+ dendritic cells capture antigens from migratory malaria sporozoites and induce CD8+ T cell responses. *PLoS Pathog.* **11**, e1004637 (2015).
43. J. Adovelande *et al.*, Detection and cartography of the fluorinated antimalarial drug mefloquine in normal and Plasmodium falciparum infected red blood cells by scanning ion microscopy and mass spectrometry. *Biol. Cell* **81**, 185–192 (1994).
44. H. Doi, A. Ishii, K. Shimono, A rapid in vitro assay system using anti-bromodeoxyuridine for drug susceptibility of Plasmodium falciparum. *Trans. R. Soc. Trop. Med. Hyg.* **82**, 190–193 (1988).
45. S. M. Man *et al.*, IRGB10 Liberates Bacterial Ligands for Sensing by the AIM2 and Caspase-11-NLRP3 Inflammasomes. *Cell* **167**, 382–396 e317 (2016).
46. R. Karki *et al.*, Concerted activation of the AIM2 and NLRP3 inflammasomes orchestrates host protection against Aspergillus infection. *Cell Host. Microbe.* **17**, 357–368 (2015).
47. R. Finethy *et al.*, Guanylate binding proteins enable rapid activation of canonical and noncanonical inflammasomes in Chlamydia-infected macrophages. *Infect. Immun.* **83**, 4740–4749 (2015).
48. P. Kalantari *et al.*, Dual engagement of the NLRP3 and AIM2 inflammasomes by plasmodium-derived hemozoin and DNA during malaria. *Cell Rep.* **6**, 196–210 (2014).
49. J. C. Kagan, V. G. Magupalli, H. Wu, SMOCs: Supramolecular organizing centres that control innate immunity. *Nat. Rev. Immunol.* **14**, 821–826 (2014).
50. S. Veeranki, X. Duan, R. Panchanathan, H. Liu, D. Choubey, IFI16 protein mediates the anti-inflammatory actions of the type-I interferons through suppression of activation of caspase-1 by inflammasomes. *PloS one* **6**, e27040 (2011).
51. N. K. Minkah, C. Schafer, S. H. I. Kappe, Humanized mouse models for the study of human malaria parasite biology, pathogenesis, and immunity. *Front. Immunol.* **9**, 807 (2018).
52. D. Boucher *et al.*, Caspase-1 self-cleavage is an intrinsic mechanism to terminate inflammasome activity. *J. Exp. Med.* **215**, 827–840 (2018).
53. M. N. Bouchlaka *et al.*, Human mesenchymal stem cell-educated macrophages are a distinct high IL-6-producing subset that confer protection in graft-versus-host-disease and radiation injury models. *Biol Blood Marrow. Transplant* **23**, 897–905 (2017).
54. J. Ignatius Irudayam *et al.*, Profile of Inflammation-associated genes during Hepatic Differentiation of Human Pluripotent Stem Cells. *Data Brief* **5**, 871–878 (2015).
55. J. I. Irudayam *et al.*, Characterization of type I interferon pathway during hepatic differentiation of human pluripotent stem cells and hepatitis C virus infection. *Stem Cell Res* **15**, 354–364 (2015).
56. H. Wang *et al.*, Myc and ChREBP transcription factors cooperatively regulate normal and neoplastic hepatocyte proliferation in mice. *J. Biol Chem.* **293**, 14740–14757 (2018).
57. S. M. Man, T. D. Kanneganti, Converging roles of caspases in inflammasome activation, cell death and innate immunity. *Nat. Rev. Immunol.* **16**, 7–21 (2016).
58. Y. Zhang, X. Chen, C. Gueydan, J. Han, Plasma membrane changes during programmed cell deaths. *Cell Res.* **28**, 9–21 (2018).
59. J. J. Hu *et al.*, FDA-approved disulfiram inhibits pyroptosis by blocking gasdermin D pore formation. *Nat. Immunol.* **21**, 736–745 (2020).

60. A. Denes, G. Lopez-Castejon, D. Brough, Caspase-1: Is IL-1 just the tip of the ICEberg? *Cell Death Dis.* **3**, e338 (2012).
61. D. C. Gowda, X. Wu, Parasite recognition and signaling mechanisms in innate immune responses to malaria. *Front. Immunol.* **9**, 3006 (2018).
62. M. M. Stevenson, E. M. Riley, Innate immunity to malaria. *Nat. Rev. Immunol.* **4**, 169–180 (2004).
63. M. Kordes, K. Matuschewski, J. C. Hafalla, Caspase-1 activation of interleukin-1beta (IL-1beta) and IL-18 is dispensable for induction of experimental cerebral malaria. *Infect. Immu.* **79**, 3633–3641 (2011).
64. L. M. N. Pereira *et al.*, Caspase-8 mediates inflammation and disease in rodent malaria. *Nat. Commun.* **11**, 4596 (2020).
65. T. Reimer *et al.*, Experimental cerebral malaria progresses independently of the Nlrp3 inflammasome. *Eur. J. Immunol.* **40**, 764–769 (2010).
66. G. Lopez-Castejon, P. Pelegrin, Current status of inflammasome blockers as anti-inflammatory drugs. *Expert Opin. Investig. Drugs.* **21**, 995–1007 (2012).
67. S. P. Kurup, R. L. Tarleton, Perpetual expression of PAMPs necessary for optimal immune control and clearance of a persistent pathogen. *Nat. Commun.* **4**, 2616 (2013).
68. L. Xu *et al.*, Mitochondrial DNA enables AIM2 inflammasome activation and hepatocyte pyroptosis in nonalcoholic fatty liver disease. *Am. J. Physiol. Gastrointest Liver Physiol.* **320**, G1034–G1044 (2021).
69. S. R. Paludan, A. G. Bowie, Immune sensing of DNA. *Immunity* **38**, 870–880 (2013).
70. M. K. Thomsen *et al.*, Lack of immunological DNA sensing in hepatocytes facilitates hepatitis B virus infection. *Hepatology* **64**, 746–759 (2016).
71. C. J. Merrick, Transfection with thymidine kinase permits bromodeoxyuridine labelling of DNA replication in the human malaria parasite Plasmodium falciparum. *Malar J.* **14**, 490 (2015).
72. E. Khanova *et al.*, Pyroptosis by caspase11/4-gasdermin-D pathway in alcoholic hepatitis in mice and patients. *Hepatology* **67**, 1737–1753 (2018).
73. A. R. Mridha *et al.*, NLRP3 inflammasome blockade reduces liver inflammation and fibrosis in experimental NASH in mice. *J. Hepatol.* **66**, 1037–1046 (2017).
74. I. Fabregat, Dysregulation of apoptosis in hepatocellular carcinoma cells. *World J. Gastroenterol.* **15**, 513–520 (2009).
75. S. Gaul *et al.*, Hepatocyte pyroptosis and release of inflammasome particles induce stellate cell activation and liver fibrosis. *J. Hepatol.* **74**, 156–167 (2020), 10.1016/j.jhep.2020.07.041.
76. J. Li *et al.*, Sorafenib inhibits caspase-1 expression through suppressing TLR4/stat3/SUMO1 pathway in hepatocellular carcinoma. *Cancer Biol. Ther.* **19**, 1057–1064 (2018).
77. W. H. Xie *et al.*, Hepatitis B virus X protein promotes liver cell pyroptosis under oxidative stress through NLRP3 inflammasome activation. *Inflamm. Res.* **69**, 683–696 (2020).
78. S. Y. Cai *et al.*, Inflammasome is activated in the liver of cholestatic patients and aggravates hepatic injury in bile duct-ligated mouse. *Cell Mol. Gastroenterol. Hepatol.* **9**, 679–688 (2020).
79. L. J. Dixon, M. Berk, S. Thapaliya, B. G. Papouchado, A. E. Feldstein, Caspase-1-mediated regulation of fibrogenesis in diet-induced steatohepatitis. *Lab Invest.* **92**, 713–723 (2012).
80. J. Li *et al.*, Blocking GSDMD processing in innate immune cells but not in hepatocytes protects hepatic ischemia-reperfusion injury. *Cell Death Dis.* **11**, 244 (2020).
81. Q. Feng *et al.*, Caspase-1alpha is down-regulated in human ovarian cancer cells and the overexpression of caspase-1alpha induces apoptosis. *Cancer Res.* **65**, 8591–8596 (2005).
82. S. Gansauge *et al.*, Interleukin 1beta-converting enzyme (caspase-1) is overexpressed in adenocarcinoma of the pancreas. *Cancer Res.* **58**, 2703–2706 (1998).
83. A. Jarry *et al.*, Interleukin 1 and interleukin 1beta converting enzyme (caspase 1) expression in the human colonic epithelial barrier. Caspase 1 downregulation in colon cancer. *Gut* **45**, 246–251 (1999).
84. C. Johansen, K. Moeller, K. Kragballe, L. Iversen, The activity of caspase-1 is increased in lesional psoriatic epidermis. *J. Invest. Dermatol.* **127**, 2857–2864 (2007).
85. P. Pasinelli, M. K. Houseweart, R. H. Brown Jr., D. W. Cleveland, Caspase-1 and -3 are sequentially activated in motor neuron death in Cu, Zn superoxide dismutase-mediated familial amyotrophic lateral sclerosis. *Proc. Natl. Acad. Sci. U.S.A.* **97**, 13901–13906 (2000).
86. K. S. Robinson *et al.*, Enteroviral 3C protease activates the human NLRP1 inflammasome in airway epithelia. *Science* **370**, eaay2002 (2020), 10.1126/science.aay2002.
87. R. N. Winter, A. Kramer, A. Borkowski, N. Kyprianou, Loss of caspase-1 and caspase-3 protein expression in human prostate cancer. *Cancer Res.* **61**, 1227–1232 (2001).
88. A. Roth *et al.*, A comprehensive model for assessment of liver stage therapies targeting Plasmodium vivax and Plasmodium falciparum. *Nat. Commun.* **9**, 1–16 (2018).
89. P. Gurung *et al.*, Chronic TLR stimulation controls NLRP3 inflammasome activation through IL-10 mediated regulation of NLRP3 expression and Caspase-8 activation. *Sci. Rep.* **5**, 14488 (2015).
90. G. Arreaza, V. Corredor, F. Zavala, Plasmodium yoelii: Quantification of the exoerythrocytic stages based on the use of ribosomal RNA probes. *Exp. Parasitol.* **72**, 103–105 (1991).
91. S. P. Kurup *et al.*, Regulatory T cells impede acute and long-term immunity to blood-stage malaria through CTLA-4. *Nat Med.* **23**, 1220–1225 (2017), 10.1038/nm.4395.
92. V. A. Rathinam *et al.*, The AIM2 inflammasome is essential for host defense against cytosolic bacteria and DNA viruses. *Nat. Immunol.* **11**, 395–402 (2010).
93. M. J. Kim, N. Ahituv, The hydrodynamic tail vein assay as a tool for the study of liver promoters and enhancers. *Methods Mol. Biol.* **1015**, 279–289 (2013).
94. E. Kummari *et al.*, Activity-based proteomic profiling of deubiquitinating enzymes in Salmonella-infected macrophages leads to identification of putative function of UCH-L5 in Inflammasome regulation. *PloS one* **10**, e0135531 (2015).
95. T. Kuriakose *et al.*, ZBP1/DAI is an innate sensor of influenza virus triggering the NLRP3 inflammasome and programmed cell death pathways. *Sci. Immunol.* **1**, aag2045 (2016).
96. R. Vijay *et al.*, Virus-induced inflammasome activation is suppressed by prostaglandin D2/DP1 signaling. *Proc. Natl. Acad. Sci. U.S.A.* **114**, E5444–E5453 (2017).